

ORIGINAL ARTICLE

Open Access



Oxygen-enhanced MRI assessment of tumour hypoxia in head and neck cancer is feasible and well tolerated in the clinical setting

Alastair McCabe^{1,2*} , Stewart Martin¹, Selene Rowe³, Jagrit Shah³, Paul S. Morgan^{4,5}, Damian Borys⁶ and Rafal Panek^{4,5}

Abstract

Background Tumour hypoxia is a recognised cause of radiotherapy treatment resistance in head and neck squamous cell carcinoma (HNSCC). Current positron emission tomography-based hypoxia imaging techniques are not routinely available in many centres. We investigated if an alternative technique called oxygen-enhanced magnetic resonance imaging (OE-MRI) could be performed in HNSCC.

Methods A volumetric OE-MRI protocol for dynamic T1 relaxation time mapping was implemented on 1.5-T clinical scanners. Participants were scanned breathing room air and during high-flow oxygen administration. Oxygen-induced changes in T1 times ($\Delta T1$) and R_2^* rates (ΔR_2^*) were measured in malignant tissue and healthy organs. Unequal variance *t*-test was used. Patients were surveyed on their experience of the OE-MRI protocol.

Results Fifteen patients with HNSCC (median age 59 years, range 38 to 76) and 10 non-HNSCC subjects (median age 46.5 years, range 32 to 62) were scanned; the OE-MRI acquisition took less than 10 min and was well tolerated. Fifteen histologically confirmed primary tumours and 41 malignant nodal masses were identified. Median (range) of $\Delta T1$ times and hypoxic fraction estimates for primary tumours were -3.5% (-7.0 to -0.3%) and 30.7% (6.5 to 78.6%) respectively. Radiotherapy-responsive and radiotherapy-resistant primary tumours had mean estimated hypoxic fractions of 36.8% (95% confidence interval [CI] 17.4 to 56.2%) and 59.0% (95% CI 44.6 to 73.3%), respectively ($p=0.111$).

Conclusions We present a well-tolerated implementation of dynamic, volumetric OE-MRI of the head and neck region allowing discernment of differing oxygen responses within biopsy-confirmed HNSCC.

Trial registration ClinicalTrials.gov, [NCT04724096](https://clinicaltrials.gov/ct2/show/study/NCT04724096). Registered on 26 January 2021.

Relevance statement MRI of tumour hypoxia in head and neck cancer using routine clinical equipment is feasible and well tolerated and allows estimates of tumour hypoxic fractions in less than ten minutes.

*Correspondence:

Alastair McCabe

alastair.mccabe@nottingham.ac.uk; alastair.mccabe@nuh.nhs.uk

Full list of author information is available at the end of the article



© The Author(s) 2024. **Open Access** This article is licensed under a Creative Commons Attribution 4.0 International License, which permits use, sharing, adaptation, distribution and reproduction in any medium or format, as long as you give appropriate credit to the original author(s) and the source, provide a link to the Creative Commons licence, and indicate if changes were made. The images or other third party material in this article are included in the article's Creative Commons licence, unless indicated otherwise in a credit line to the material. If material is not included in the article's Creative Commons licence and your intended use is not permitted by statutory regulation or exceeds the permitted use, you will need to obtain permission directly from the copyright holder. To view a copy of this licence, visit <http://creativecommons.org/licenses/by/4.0/>.

Key points

- Oxygen-enhanced MRI (OE-MRI) can estimate tumour hypoxic fractions in ten-minute scanning.
- OE-MRI may be incorporable into routine clinical tumour imaging.
- OE-MRI has the potential to predict outcomes after radiotherapy treatment.

Keywords Head and neck neoplasms, Magnetic resonance imaging, Oxygen, Radiotherapy, Tumour hypoxia

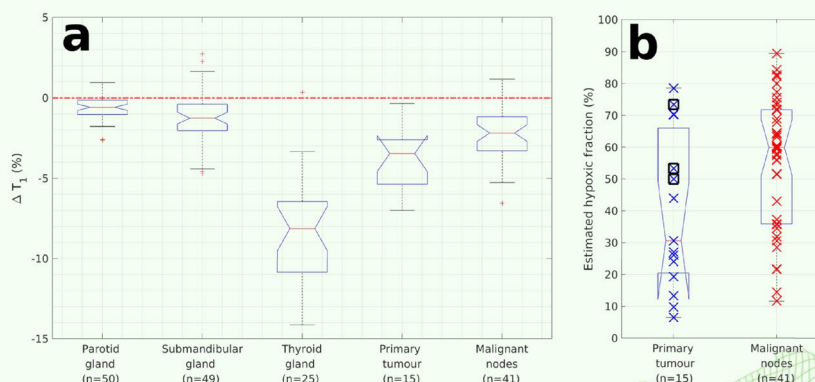
Graphical Abstract

Oxygen-enhanced MRI assessment of tumour hypoxia in head and neck cancer is feasible and well tolerated in the clinical setting

ESR[®] EUROPEAN SOCIETY OF RADIOLOGY

- Oxygen-enhanced MRI may be incorporable into routine clinical head and neck tumour imaging.
- Oxygen-enhanced MRI has potential to predict outcomes from radiotherapy treatment

Box plots of oxygen induced ΔT_1 times (a) and hypoxic fraction estimates (b) - radioresistant tumours surrounded by black box.



OE-MRI in head and neck cancer on a clinical scanner can estimate tumour hypoxic fractions with less than 10-min scanning.

European
Radiology
EXPERIMENTAL

Eur Radiol Exp (2024) McCabe A, Martin S, Rowe S et al.
DOI: 10.1186/s41747-024-00429-1

Background

Head and neck cancer is the eighth most common cancer in the UK [1] with the majority of tumours being head and neck squamous cell carcinomas (HNSCC). Survival rates vary by location with hypopharyngeal tumours having 5-year survival rates of only 27% [2]. Treatment approaches include surgical resection or radical radiotherapy with or without chemotherapy. Low levels of oxygen within malignant tissue (tumour hypoxia) are a well-recognised cause of local treatment failure in HNSCC treated with radical radiotherapy [3, 4]. Hypoxia modification strategies such as boost doses of radiation to hypoxic tumour regions [5, 6] have yet to garner routine clinical use in part due to the lack of readily accessible methods of determining and mapping tumour hypoxia [7, 8].

The most widely used hypoxia imaging technique is hypoxic positron emission tomography (PET), primarily performed with [¹⁸F]-labelled nitromidazole compounds [9]. Hypoxia-PET has been studied in HNSCC [10–16] and shown capable of predicting clinical outcomes [11, 13]; however, it requires an additional dedicated imaging session, can cost substantially more per scan than alternative clinical imaging techniques [17], and is not routinely available in most UK oncology centres.

Oxygen-enhanced magnetic resonance imaging (OE-MRI) is an alternative hypoxic imaging technique that maps tissue oxygenation based upon changes in the longitudinal relaxation rate R_1 ($1/T_1$) following the delivery of supplemental oxygen [18]. In well-oxygenated tissues, supplemental oxygen increases the concentration of dissolved oxygen due to the near-complete saturation of haemoglobin

causing an increase in tissue R_1 rates (decrease in T1 times) due to the paramagnetic properties of dissolved oxygen [19]. Conversely, in hypoxic tissues, additional oxygen preferentially alters the deoxyhaemoglobin to oxyhaemoglobin ratio with minimal alteration in plasma oxygen concentrations. T1 times in hypoxic regions are therefore relatively invariant to supplemental oxygen challenge [19–21].

Due to a lack of correlation between tumour averaged oxygen-induced T1 changes and reference hypoxia indicators [19, 21–25], previous OE-MRI studies have suggested combining OE-MRI with additional metrics such as tumour perfusion assessments [19] or blood oxygen level-dependent (BOLD) measurements [24, 26, 27]. BOLD refers to the reduction in R_2^* rate with the reduction in deoxyhaemoglobin to oxyhaemoglobin ratio as occurs in perfused hypoxic regions following an oxygen challenge. As R_1 relaxation rates are also proportional to deoxyhaemoglobin concentrations [28], the addition of BOLD measurements to T1-based OE-MRI may refine the characterisation of the oxygenation status of tumours [24, 27].

The aims of this research were to assess if it is feasible to perform OE-MRI on a clinical scanner as part of a routine clinical imaging session in patients with HNSCC and if the addition of oxygen-induced ΔR_2^* measurements changes the categorisation of HNSCC oxygenation status. In addition, we sought to formally assess the tolerability of OE-MRI in patients with HNSCC and test differences between OE-MRI-derived parameters and clinical outcomes for patients treated with curative intent radiotherapy.

Methods

All participants were prospectively recruited between August 2021 and November 2022 after research ethics approval (South Central Berkshire Research Ethics Committee, reference 21/SC/0050, 9 February 2021) and provided written informed consent (ClinicalTrials.gov identifier NCT04724096). Patient participants were identified prior to a clinically indicated neck MRI for the staging of suspected HNSCC by consultant surgeons on the national otolaryngology specialist register (minimum four-year experience). Histological diagnosis was not required prior to scanning if there was a strong clinical suspicion of HNSCC, reflecting the clinical diagnostic pathway at our institution. All primary tumours were confirmed as squamous cell carcinoma based on routine histopathological analysis of core biopsy specimens as per the clinical institutional procedures. Oropharyngeal primary tumours were tested for evidence of human papillomavirus (HPV) as per the local clinical protocols via *in situ* hybridisation for HPV deoxyribonucleic acid using the INFORM HPV III Family 16 Probe (Ventana Medical Systems, Tucson, AZ, USA).

Participants were scanned on Magnetom Sola 1.5-T scanners (Siemens Healthineers, Erlangen, Germany) wearing an adult nonbreathing mask with a reservoir bag with the study protocol performed immediately prior to a routine clinical scan for patient participants. A safety valve allowed the wearing of the mask without supplemental gas delivery meaning patients could be switched from breathing room air to 15 L/min high-flow oxygen without requiring re-positioning or the use of a gas

Table 1 Acquisition parameters for the study sequences

Sequence name	qDixon	VIBE
Sequence type	3D multi-echo Dixon	3D spoiled gradient-echo
Orientation	Axial	Axial
Repetition time (ms)	15.6	10 (4.2)
Echo time (ms)	Range 1.10 to 14.28 with 12 echoes	1.27 (1.48)
Flip angle (°)	4	2/18
Bandwidth (Hz/pixel)	1,090	399 (313)
Matrix	96×96	128×128
Field of view (mm ²)	200×200	200×200
Slice thickness (mm)	2.5	2.5
Number slices	72	72
Number acquisitions	1 pre- and post-oxygen	Proton density: 3 (5) Dynamic: 40 (60)
Oxygen on (min:s)	-	3:32 (2:09)
Total acquisition time (min:s)	0:58	8:27 (5:35)
Time for single acquisition (s)	29	11.8 (5.15)

Values in parentheses represent the initial imaging protocol reviewed after the first three nonpatient volunteers and two patients

3D Three-dimensional

mixer. The posterior component of the head coil together with an ultraflex large 18-channel coil positioned over the neck region was used to facilitate the comfortable placement of the oxygen mask (Supplementary Fig. S1). Examinations were performed by state-registered clinically employed specialised radiographers (minimum one-year experience) as a component of patients’ routine clinical imaging appointments. Oxygen administration was supervised by a clinical oncologist (two-year experience).

An initial T2-weighted sequence was performed to aid study sequence planning. All subsequent research sequences were acquired with identical field of view without repositioning the participant. R_2^* mapping was performed on room air and repeated after dynamic T1 mapping using a manufacturer-supplied multi-echo Dixon protocol (qDixon, Table 1). Dynamic T1 mapping was performed using the sequential acquisition of three-dimensional spoiled gradient echo volumetric interpolated breath-hold examination (VIBE) sequence. Following an image quality review after the first three nonpatient volunteers and two patients, the VIBE sequence was modified to increase the signal-to-noise ratio (Table 1). The resulting sequence was used for the subsequent 20 participants (2 nonpatient volunteers and 18 patients) with the overall OE-MRI acquisition taking 9:25 min:s (Fig. 1). The total air/oxygen breathing VIBE periods were 3:32 and 4:55 min:s, respectively. The VIBE temporal resolution was 11.8 s.

VIBE images were corrected for motion via nonrigid registration (using Advanced Normalization Tools [29]). The water image from the qDixon sequence was similarly registered for each participant and the resulting registration transformation was applied to derived qDixon parametric maps.

A four-dimensional median filter was applied to dynamic images before producing voxel-wise T1 maps for each dynamic acquisition using the variable flip angle–VFA methodology [30]. An initial room air period

was defined from 0:35 to 3:32 min:s and hyperoxic phase from 5:30 min:s until the end of the dynamic sequence. Mean voxel-wise room air T1 times ($T1_{Air}$) and hyperoxic T1 times ($T1_{O_2}$) were determined and voxel-wise changes in T1 times defined as:

$$\Delta T1(voxel) = \frac{T1_{O_2} - T1_{Air}}{T1_{Air}} \times 100\%$$

Image processing was performed using in-house software developed in MATLAB version R2018b (Mathworks, Natick, MA, USA) by a clinical oncologist (two-year experience) and an MRI physicist (over ten-year experience). The stability of the T1 mapping sequence was assessed using a Eurospin TO5 phantom with twelve gel-filled tubes with varying T1 relaxation times [31]. T1 times were determined for volumes of interests (VOIs) on the central slice for each tube using identical methodology to the clinical experiments. Coefficients of variation over the study dynamic sequence were determined for each tube.

Histologically confirmed primary tumours were contoured on initial VIBE images. Malignant nodes were defined as nodal masses in patients with biopsy-proven HNSCC whose radiological appearance was deemed malignant by the local head and neck multidisciplinary team. Contoured volumes less than 0.25 mL were excluded. Parotid, submandibular, and thyroid glands were contoured in accordance with radiotherapy contouring guidelines [32]. All contouring was performed using ITK-SNAP (version 3.4.0) [33] by a clinical oncologist (two-year experience).

Average VOI $\Delta T1$ times and ΔR_2^* rates were defined as the median of $\Delta T1(voxel)$ times and voxel R_2^* rate differences with statistical significance against the null hypothesis of no change in median value assessed via Wilcoxon signed-rank test, with p -values lower than 0.05 as significant. Individual voxels within VOIs were interrogated for significant $\Delta T1$ via a two-tailed unequal variance t -test,

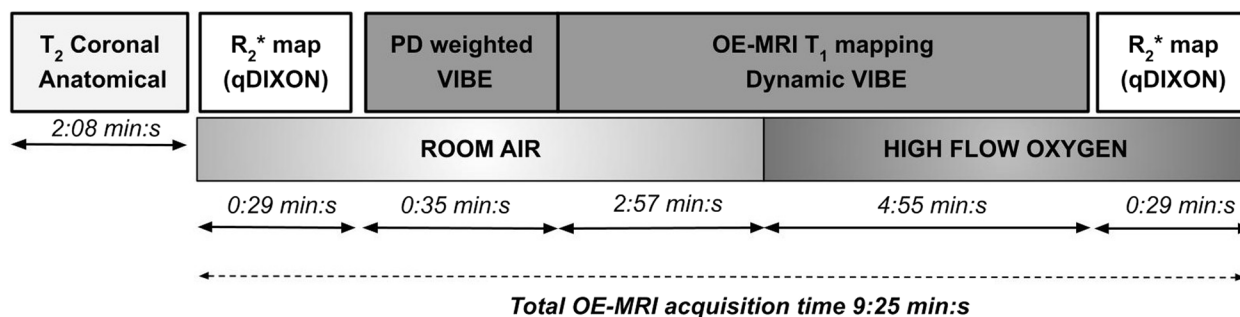


Fig. 1 Study sequences and timing of switch from room air to high flow oxygen. Sequence parameters provided in Table 1. OE-MRI Oxygen-enhanced magnetic resonance imaging, VIBE Volumetric interpolated breath-hold examination

with p -values lower than 0.05 as significant. Estimates of hypoxic fractions were defined as the percentage of voxels not showing statistically significant negative ΔT_1 . Parcellation analysis of primary tumours and malignant nodes was performed using VOI averaged ΔT_1 times and ΔR_2^* rates [24]. Statistical analysis was performed using MATLAB version R2018b by a clinical oncologist (two-year experience) and an MRI physicist (over ten-year experience).

All patient participants were surveyed on their scan experience using an MRI-specific anxiety questionnaire [34]. Patients were asked to complete two copies of the questionnaire pertaining to the study protocol and routine clinical scan. Paired scores were compared using the Wilcoxon signed-rank test, with p -values lower than 0.05 as significant.

Patients with histologically confirmed HNSCC were discussed at the local head and neck multidisciplinary meeting and received treatment at a single centre in accordance with local protocols. Twelve weeks following the completion of curative intent radiotherapy, patients underwent an ^{18}F -fluoro-2-deoxy-D-glucose-PET scan [35]. Primary tumours with a complete metabolic response were classed as responders. Nonresponders had subsequent management decided upon by the local head and neck multidisciplinary team. Patients' treatment and follow-up were unaffected by the study. Estimated hypoxic fractions and VOI averaged ΔT_1 were compared for responding and

nonresponding groups via two-tailed unequal variance t -test, with p -values lower than 0.05 as significant.

Results

Temporal stability assessment of the dynamic VIBE T1 mapping protocol showed median (range) coefficients of variation 0.2% (0.1 to 0.4%) (Supplementary Fig. S2).

Five nonpatient volunteers (median age 32 years, range 31 to 60) and 20 patients with suspected HNSCC (median age 57 years, range 36 to 76) were recruited of whom 15 received histological diagnoses of HNSCC (median age 59 years, range 38 to 76). Out of the 5 patients who did not have HNSCC, 1 had a lymphoepithelial cyst (patient 2), 1 had benign cystic lesion (patient 18), and 3 had no radiological abnormality identified (patients 8, 12, 17). Adequate inflation of the mask nonrebreather bag was recorded for all participants. One patient (patient ID 12) terminated the study early following dynamic acquisition 32. ΔT_1 maps were produced with the hyperoxic phase defined using the final seven dynamic measurements.

Normal structures

OE-MRI data from all 25 participants was used to determine VOI averaged ΔT_1 times for normal structures in the head and neck region. Median (range) ΔT_1 times were -0.6% (-2.6 to 1.0%) for parotid glands, -1.3% (-4.7 to 2.7%) for submandibular glands and -8.1% (-14.1 to 0.4%) for thyroid glands (Fig. 2). Figure 3 shows example ΔT_1

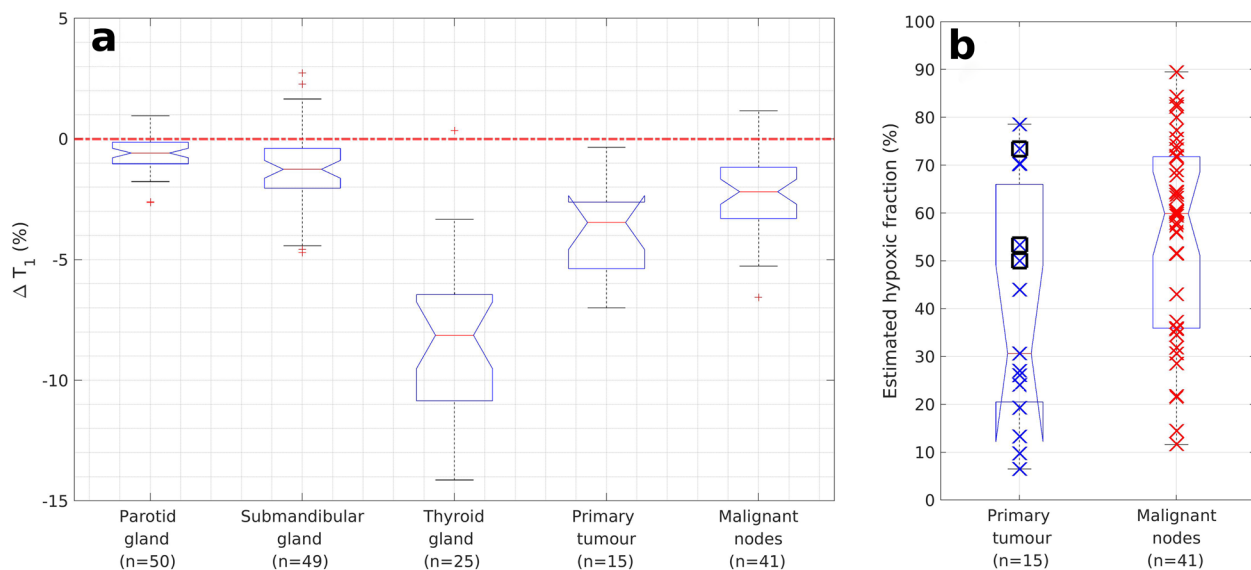


Fig. 2 **a** Notched box plots of oxygen-induced ΔT_1 (%) times for all 25 participants for the parotid, submandibular, and thyroid glands and for the 15 patients with head and neck squamous cell carcinoma for the primary tumour and malignant nodal masses. The single outlier point showing positive ΔT_1 in the thyroid gland came from a nonpatient volunteer. **b** Notched box plots with overlaid data points of estimates of hypoxic fractions (%) for malignant tissues. Data points corresponding to primary tumours with evidence of residual disease post-radiotherapy treatment are surrounded by a black box

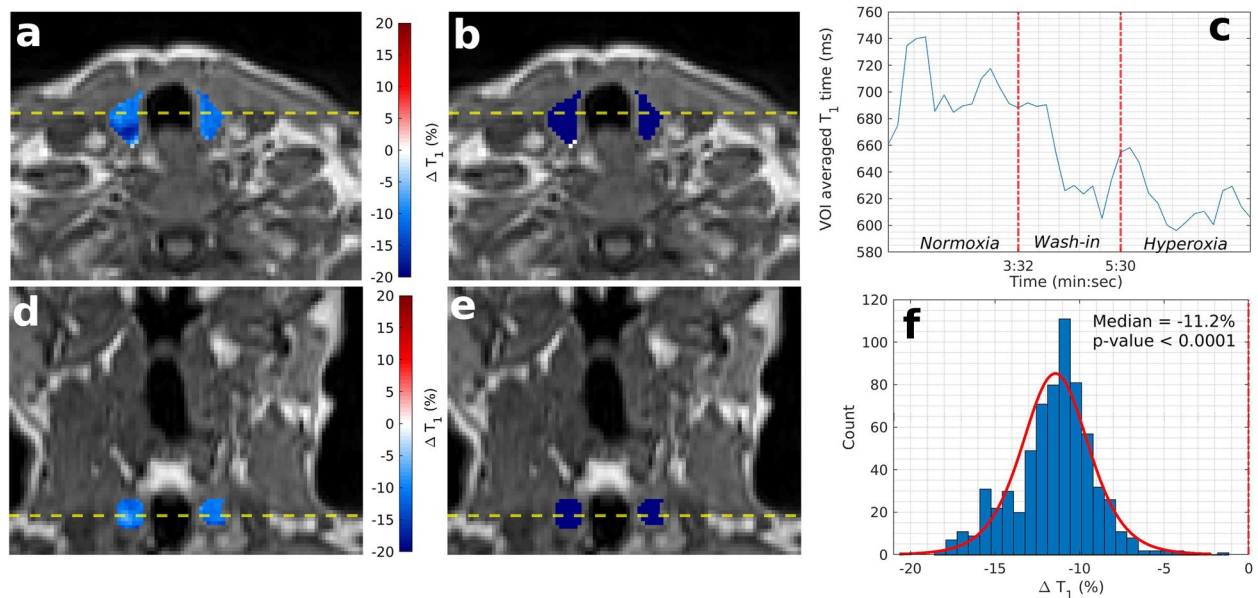


Fig. 3 Example OE-MRI parametrical maps of thyroid gland (patient number 5). T1 weighted VIBE image is shown with overlaid parametric ΔT_1 map of the thyroid gland (**a, d**, axial and coronal plane respectively) and overlaid statistical map of ΔT_1 times (**b, e**). Blue colour indicates statistically significant decrease in T1 times, white indicates no statistically significant change, and red indicates statistically significant increasing T1 times. **c** Time series of T1 times averaged over the entire thyroid VOI. **f** Histogram of ΔT_1 times for the entire thyroid VOI. *OE-MRI* Oxygen-enhanced magnetic resonance imaging, *VIBE* Volumetric interpolated breath-hold examination, *VOI* Volume of interest

Table 2 Characteristics of the squamous cell carcinomas for the 15 patients with histologically confirmed tumours

Patient number	Sex	Age (years)	Smoking	Site	Stage (TNM8)	p16	HPV DNA	Primary size (mL)	Lymph node masses	
									Number	Size (mL) Median (range)
1	M	54	Never	Palatine tonsil	T4aN2b	-	N/A	31.15	2	1.90 (1.31–2.50)
3	M	45	Current	Pyriiform fossa	T2N2b	N/A	N/A	4.35	2	7.04 (4.27–9.81)
4	M	69	Ex	Oropharynx	T0N2	+	+	-	1	10.71
5	M	66	Never	Pyriiform fossa	T2N1	+	+	3.98	2	6.26 (1.64–10.88)
6	M	46	Current	Nasopharynx	T1N2	N/A	N/A	8.83	10	2.60 (1.01–20.56)
7	M	66	Ex	Base of tongue	T4aN2	+	N/A	33.70	4	1.83 (0.37–6.44)
9	M	62	Never	Base of tongue	T1N1	+	+	1.31	1	11.98
10	M	55	Current	Base of tongue	T3N1	+	+	5.04	2	2.90 (0.26–5.55)
				Palatine tonsil	T3N0	+	+	17.69	-	-
11	M	72	Ex	Pyriiform fossa	T4aN1	N/A	N/A	33.11	1	0.46
13	F	59	Current	Vallecula	T1N2c	-	-	0.54	1	9.94
14	M	56	Current	Palatine tonsil	T4aN2b	+	-	21.60	3	1.10 (0.48–8.40)
15	M	38	Current	Palatine tonsil	T1N1	+	+	2.35	7	2.62 (0.54–7.19)
16	M	65	Never	Palatine tonsil	T2N1	+	N/A	3.75	2	6.00 (0.93–11.07)
19	F	76	Never	Palatine tonsil	T2N1	+	+	4.55	1	8.35
20	M	57	Current	Larynx	T3N2b	N/A	N/A	7.20	2	1.52 (1.17–1.87)
		Median (range)						5.04 (0.26–33.70)	2 (1–10)	2.62 (0.26–20.56)
		Total number of lesions						15	41	-

All histology and staging were discussed at the local head and neck cancer multidisciplinary team meeting

HPV DNA Human papillomavirus deoxyribonucleic acid, N/A Not assessed

parametric maps, VOI averaged T1 time series, and total VOI ΔT_1 histogram for an example thyroid gland.

Malignant tissue

Fifteen primary tumours (median volume 5.04 mL, range 0.54 to 33.70 mL) and 41 distinct malignant nodal masses (median volume 2.62 mL, range 0.26 to 20.56 mL) were contoured (Table 2).

Median (range) ΔT_1 times were -3.5% (-7.0 to -0.3%) for primary tumours and -2.2% (-6.5 to 1.2%) for malignant nodes. Median (range) estimated hypoxic fractions for primary tumours and malignant nodes were 30.7% (6.5 to 78.6%) and 59.9% (11.6 to 89.5%) respectively (Fig. 2). HPV-related and unrelated oropharyngeal cancers had median (range) estimated hypoxic fractions of 25.6% (6.5 to 70.2%) and 52.4% (26.1 to 78.6%) respectively. Figures 4 and 5 show example ΔT_1 parametric maps, VOI averaged T1 time series, and total VOI ΔT_1 histograms for example primary tumours with low and high estimated hypoxic fractions respectively (full data in Additional file 1: Appendix 1).

Out of 15 patients with confirmed HNSCC, 11 (73%) proceeded to curative intent radiotherapy and 9 underwent post-treatment ^{18}F -fluoro-2-deoxy-D-glucose-PET scan (1 patient had post-treatment MRI scan). Of these

10 primary tumours, 7 (70%) were responders, with 3 (30%) showing residual disease, confirmed histologically in 2 cases (Table 3). Mean estimated hypoxic fractions were 36.8% (95% confidence intervals [CI] 17.4 to 56.2%) and 59.0% (95% CI 44.6 to 73.3%) for responding and nonresponding primary tumours respectively ($p=0.111$, unequal variance t -test). VOI mean ΔT_1 values were -3.8% (95% CI -5.6 to -2.0%) for responding and -3.1% (95% CI -3.5 to -2.6%) for residual disease ($p=0.484$, unequal variance t -test).

R_2^* measurements were obtained in all participants. Median (range) ΔR_2^* rates were 0.4 Hz (-29.1 to 10.7 Hz) for primary tumours and 0.2 Hz (-12.7 to 24.7 Hz) for malignant nodes (Fig. 6). In patients who had curative intent radiotherapy, mean ΔR_2^* rates were 6.3 Hz (95% CI 1.9 to 10.7 Hz) and -1.7 Hz (95% CI -8.8 to 5.4 Hz) for responding and radiotherapy-resistant primary tumours ($p=0.812$, unequal variance t -test) with baseline mean R_2^* rates of 33.3 Hz (95% CI 15.0 to 51.5 Hz) and 44.8 Hz (95% CI 42.3 to 47.3 Hz) respectively ($p=0.897$, unequal variance t -test).

Anxiety questionnaire

All 20 patients completed the anxiety questionnaire with 40% (8/20) stating they had undergone an MRI scan

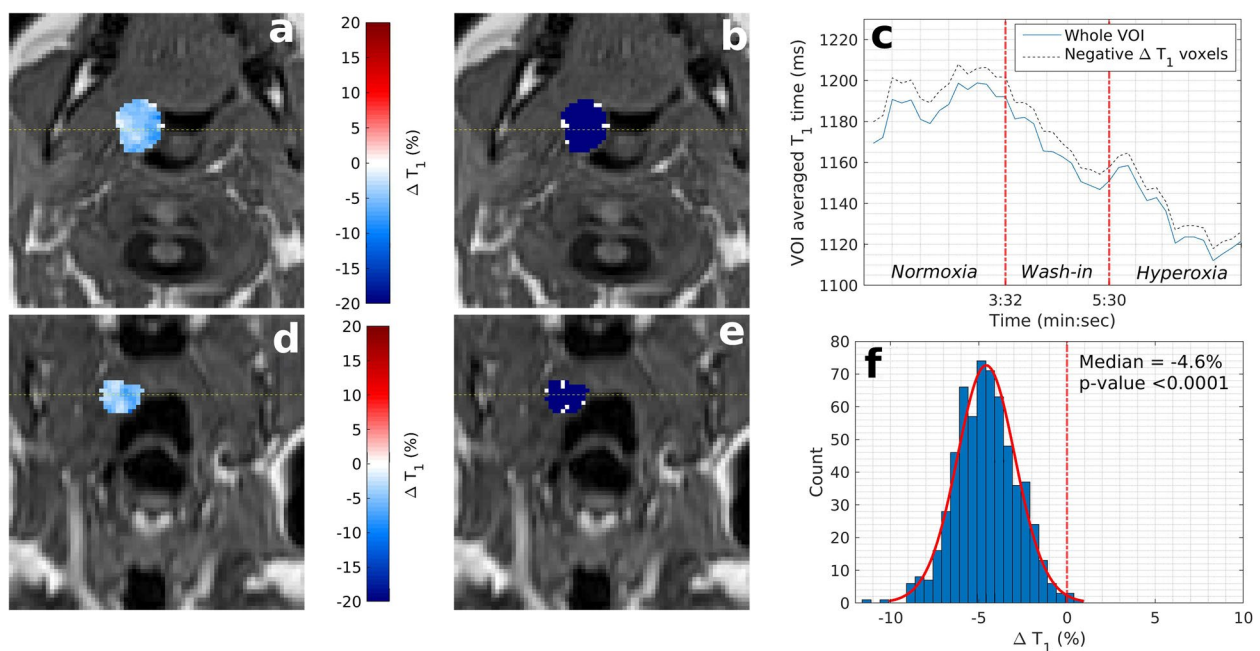


Fig. 4 Example OE-MRI parametrical maps in a primary tumour with a complete response to radiotherapy treatment (patient number 16). Low estimated hypoxic fraction (9.8%) is shown on a T1-weighted VIBE image with overlaid parametric ΔT_1 map of the primary tumour (**a, d**, axial and coronal plane, respectively) and overlaid statistical map of ΔT_1 times (**b, e**). Blue colour indicates a statistically significant decrease in T1 times, white indicates no statistically significant change, and red indicates statistically significant increasing T1 times. **c** Time series of T1 times averaged over the entire primary tumour VOI and over those voxels with significantly decreasing T1 times only. **f** Histogram of ΔT_1 times for the entire primary tumour VOI. OE-MRI Oxygen-enhanced magnetic resonance imaging, VIBE Volumetric interpolated breath-hold examination, VOI Volume of interest

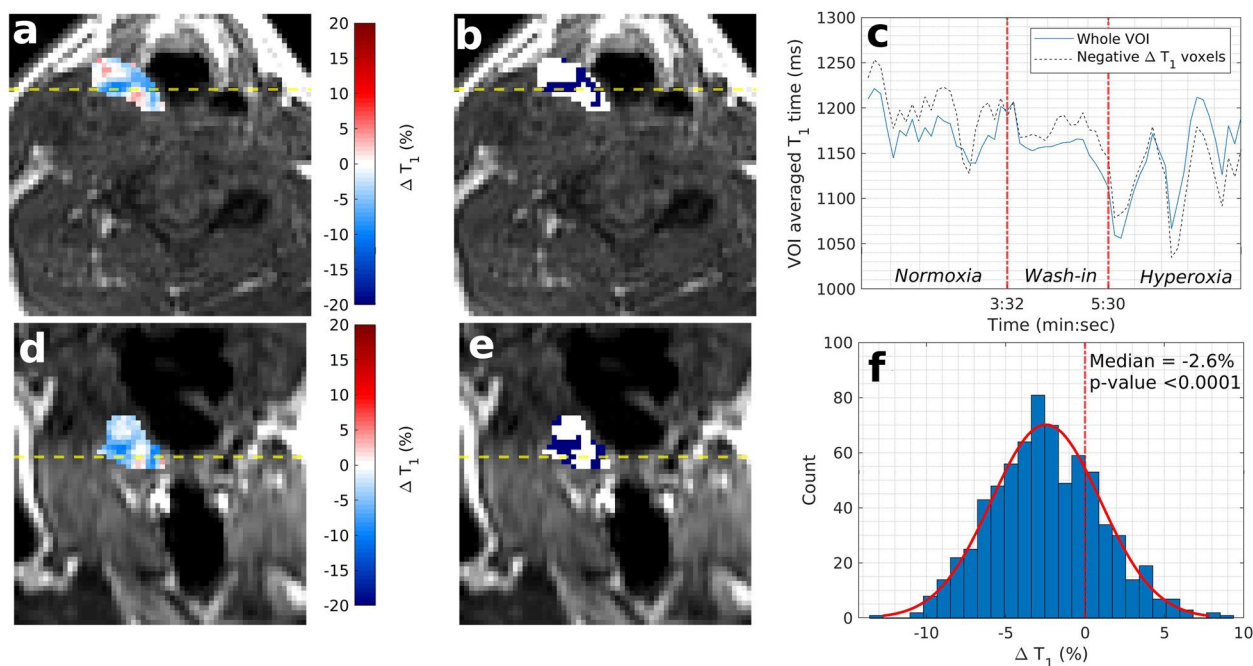


Fig. 5 Example OE-MRI parametrical maps in a patient with a primary tumour with residual disease post radiotherapy treatment (patient number 3). High estimated hypoxic fraction (73.5%) is shown on a T1-weighted VIBE image with overlaid parametric ΔT_1 map of the primary tumour (**a, d**, axial and coronal plane, respectively) and overlaid statistical map of ΔT_1 times (**b, e**). Blue colour indicates a statistically significant decrease in T1 times, white indicates no statistically significant change, and red indicates statistically significant increasing T1 times. **c** Time series of T1 times averaged over the entire primary tumour VOI and over those voxels with significantly decreasing T1 times only. **f** Histogram of ΔT_1 times for the entire primary tumour VOI. OE-MRI Oxygen-enhanced magnetic resonance imaging, VIBE Volumetric interpolated breath-hold examination, VOI/Volume of interest

previously. Questionnaire scores can range between 15 (lowest anxiety) and 60 (maximal anxiety) [36]. Median anxiety scores were 19.5 (range 15 to 42) and 15.5 (range 15 to 45) for study and routine scans respectively ($p=0.026$ Wilcoxon signed rank). The mean difference in anxiety scores (study minus clinical scan) was +1.5 (standard deviation 3.0, Fig. 7 and Supplementary Table S1).

Discussion

Our OE-MRI protocol was designed to be added to a standard clinical protocol using routinely available equipment therefore making this a low-cost and rapidly translatable method of hypoxia imaging in HNSCC. For this reason, we elected to use room air as opposed to medical air for the pre-oxygen acquisitions in order to avoid the need for a medical gas supply and additional equipment in the form of gas mixers. Although this meant participants did not have the opportunity to become accustomed to the gas delivery before oxygen was commenced, we did not encounter any apparent disadvantages from this approach. Despite the OE-MRI sequence taking less than ten minutes, it was possible

to image the entire tumour volume and discern differing responses to supplemental oxygen challenge.

Normal structures

The magnitude of oxygen-induced T1 shortening in parotid and submandibular glands is small indicating limited sensitivity of the OE-MRI technique in these structures. In contrast, the thyroid gland showed strong and consistent negative ΔT_1 . As OE-MRI relies on the absence of T1 shortening to determine hypoxic regions, a clinically relevant quality control structure to ensure adequate oxygen delivery to organs is desirable [18, 21, 25]. We suggest the thyroid gland may represent such a structure in the head and neck.

Malignant tissue

There is limited data in the literature on oxygen-induced ΔT_1 times in patients with HNSCC. A single study at 1.5 T reported mean oxygen-induced ΔR_1 rates of 0.019/s in six patients with HNSCC on a diagnostic MRI system, corresponding to ΔT_1 of -2.1% which is comparable

Table 3 Treatment details and outcomes of post-treatment imaging for the 15 patient participants with histologically confirmed squamous cell carcinoma

Patient number	Treatment intent	Modality	Treatment details	Post-treatment imaging outcome
1	Palliative	RT	-	N/A
3	Curative	RT	65.1Gy in 30#	MRI scan - Residual disease in primary and nodes (no biopsy undertaken).
4	Palliative	SACT	-	N/A
5	Curative	CRT	70Gy in 35# Cisplatin 40mg/m ² weekly	Complete response (FDG-PET).
6	Curative	CRT	70Gy in 35# Cisplatin 40mg/m ² weekly	Complete response (FDG-PET).
7	Curative	CRT	65.1Gy in 30# Carboplatin AUC 1.5 weekly	Residual disease in primary (FDG-PET and biopsy confirmed). Distant metastatic disease.
9	Curative	CRT	70Gy in 35# Cisplatin 40mg/m ² weekly	Complete response (FDG-PET).
10	Curative	CRT	70Gy in 35# Cisplatin 40mg/m ² weekly	Died before post-treatment scan.
11	Curative	Surgery	-	N/A
13	Curative	CRT	70Gy in 35# Cisplatin 40mg/m ² weekly	Complete response (FDG-PET).
14	Curative	CRT	70Gy in 35# Cisplatin 40mg/m ² weekly	Complete response (FDG-PET).
15	Curative	CRT	70Gy in 35# Cisplatin 40mg/m ² weekly	Complete response in primary but distant metastatic disease (FDG-PET).
16	Curative	CRT	70Gy in 35# Cisplatin 40mg/m ² weekly	Complete response (FDG-PET).
19	Curative	Surgery	-	N/A
20	Curative	CRT	70Gy in 35# Cisplatin 40mg/m ² weekly	Residual disease in primary (FDG-PET and biopsy confirmed). New malignant node outside treatment field.

Radiotherapy dose presented is delivered to the region containing the primary tumour. Post-treatment imaging was completed for 10 patients with one of them having an MRI scan rather than an FDG-PET scan due to the clinical circumstances. Highlighted rows indicate those patients with residual disease in the primary tumour on post-treatment imaging

CRT Concurrent chemoradiotherapy, FDG-PET¹⁸F-fluorodeoxyglucose positron emission tomography, RT Radiotherapy, SACT Systemic anticancer therapy

to the median primary tumour VOI ΔT_1 of -3.5% in this study. All 15 primary tumours in the current study showed statistically significant shortening of VOI median ΔT_1 times mirroring the observed oxygen-induced prolongation of all VOI averaged ΔR_1 rates in the previous 1.5-T study [37]. In contrast, a study at 3-T in five patients with oropharyngeal cancers reported tumour ΔR_1 rates ranging from -0.001 to 0.108/s with two of the mean baseline R_1 rates failing to show statistically significant change with oxygen [38].

Although our study and the previous two studies all used volumetric acquisitions, the 3-T study by Bluemke et al. [38] made single T1 measurements before and after oxygen to determine tumour ΔR_1 rates whereas our study

and that of the previous 1.5-T study by Dubec et al. [37] used dynamic acquisitions with multiple T1 measurement time points before and after oxygen administration. These dynamic measurements allow voxel-wise oxygen-induced $\Delta T_1/\Delta R_1$ maps to be produced following image coregistration to control for participant motion. Bluemke et al. [38] acknowledge that patient motion was a significant difficulty encountered in their study and focus their OE-MRI analysis on describing oxygen-induced changes to tumour region of interest R_1 histograms. We feel that dynamic OE-MRI acquisitions with appropriate image registration allow greater characterisation of tumour oxygenation status; however, standardisation of imaging parameters and data processing approaches is clearly

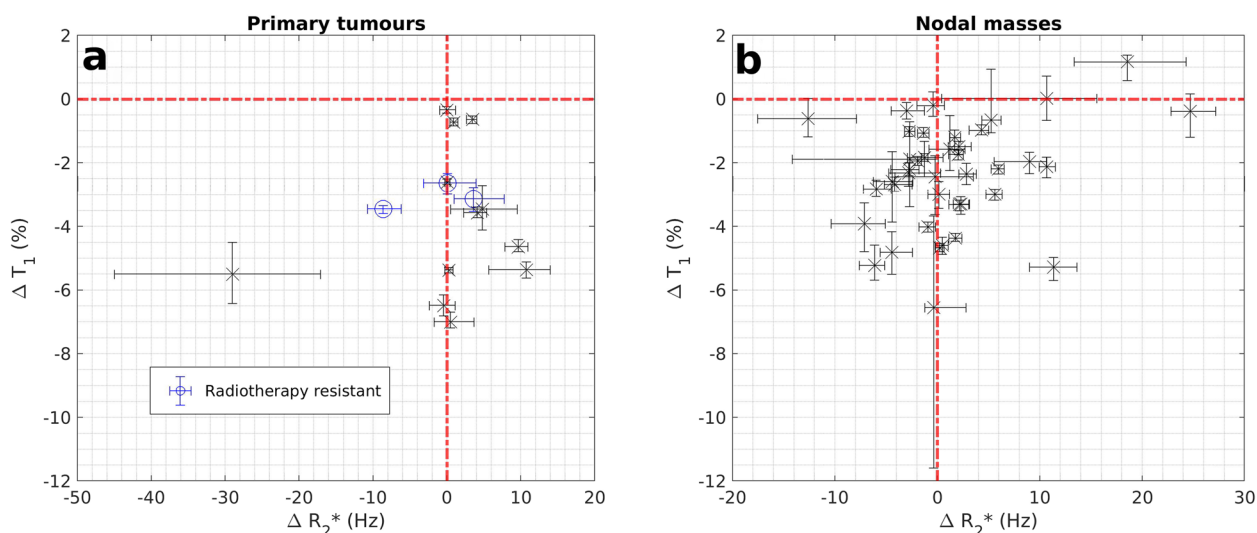


Fig. 6 Scatter plot showing categorisation of hypoxia status of primary tumours (a) and malignant nodes (b) based on VOI average median ΔT_1 times and ΔR_2^* rates with error bars indicating estimates of 95% confidence intervals derived from Bootstrap sampling with 1,000 samples. Data points corresponding to primary tumours with evidence of residual disease post-radiotherapy treatment are shown with blue circles. VOI/Volume of interest

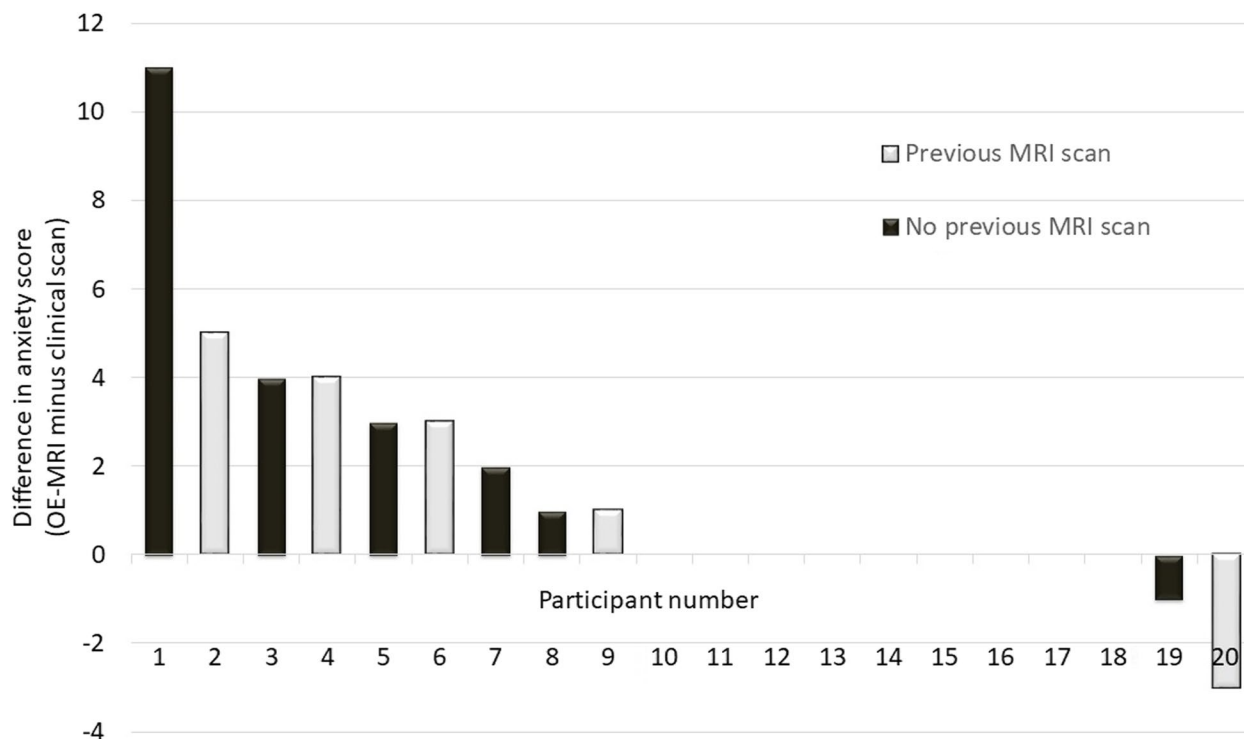


Fig. 7 Waterfall plot showing the difference in individual participant anxiety scores between the OE-MRI scan and the routine clinical scan grouped by whether they had undergone a previous scan (of any anatomical region). Higher scores indicate worse anxiety. OE-MRI Oxygen-enhanced magnetic resonance imaging

required for ready comparison of OE-MRI studies [39] as has been developed in other quantitative MRI techniques [40, 41].

The presence of hypoxia in HNSCC is well documented with oxygenation levels measured invasively using Eppendorf oxygen tension (pO_2) histography showing overall median tumour pO_2 of 10 mmHg corresponding to median hypoxic fractions of 21% and 32% depending upon the threshold set to define radiobiologically significant hypoxia (2.5 mmHg and 5 mmHg, respectively) [42]. PET-based imaging assessments of tumour hypoxia in HNSCC have shown significant interlesion variability with individual tumour fractional hypoxia estimates ranging from 0 to 95% and study population median values ranging from 0.9 to 66% [10–12, 16]. In our study, estimated hypoxic fractions also show significant interlesion variability but the median estimated hypoxic fraction in primary tumours of 31% is comparable to direct measurements.

In our study, radiotherapy nonresponding tumours show a 29.3% greater average hypoxic fraction than responding tumours, albeit not statistically significant potentially due to the sample size of this pilot study. There was no difference found with VOI averaged $\Delta T1$ times between responding and nonresponding tumours. This is in keeping with OE-MRI studies in other tumour sites which have failed to identify correlations between spatially averaged changes in $T1/R_1$ values and reference hypoxia markers [39]. Hypoxia-imaging biomarkers that capture information pertaining to the distribution of hypoxic regions are therefore likely to prove the most clinically relevant.

The dichotomisation of a voxel's hypoxic status based on the lack of statistically significant $T1$ shortening is clearly an oversimplification of the underlying continuously varying oxygen tension present in tumours. The relationship between $T1$ times and tumour pO_2 is dependent on a number of physical and physiological variables meaning it is not possible to readily ascribe pO_2 values to imaged voxels [28]. Consequently, it is not possible to state the effective pO_2 threshold for the estimates of hypoxic fractions presented in this study. The magnitude of our hypoxic fractions may be overestimated due to the inclusion of any cystic, necrotic, or nonperfused areas in the VOI [19] as well as a consequence of the study power returned from performing individual voxel analysis on a limited number of dynamic data points. This power could be increased at the expense of scan time or with the use of higher scan acceleration.

The OE-MRI sequence was developed for in-plane and slice resolution to be adequate to facilitate the fusion of acquired parametric maps to radiotherapy planning computed tomography scans with the ambition of mapping

tumour hypoxia distributions to assist in radiotherapy volume delineation. Although the spatial resolution used in this study ($1.6 \times 1.6 \times 2.5 \text{ mm}^3$) is higher than other clinical OE-MRI studies [39], it is still significantly coarser than the typical diffusion distance of molecular oxygen ($\sim 100 \text{ }\mu\text{m}$ [8]). Although the image resolution used here may detect greater levels of variability in oxygen distribution compared to coarser acquisitions, this comes at the cost of a worse signal-to-noise ratio, which may reduce the ability to discern borderline normoxic voxels thus overestimating tumour hypoxic burden.

It has been suggested that negative oxygen-induced ΔR_2^* rates may occur in hypoxic tumours due to decreases in deoxyhaemoglobin concentrations with supplemental oxygen and could potentially discriminate lower levels of hypoxia from normoxia in tumours with oxygen-induced $T1$ shortening [24, 27]. We identified two primary tumours that showed such a decrease in ΔR_2^* rates but only one of the three radiotherapy-resistant HNSCC primary tumours had such a change. In addition, we did not identify any statistically significant difference in R_2^* parameters between radiotherapy-responsive and radiotherapy-resistant primary tumours. The relationship between oxygen-induced $\Delta T1$ times, ΔR_2^* rates, and baseline R_2^* is known to be complex, in part due to potential spatial fluctuations in perfusion. As such, spatially averaged ΔR_2^* rates may not be sensitive enough to offer useful insights on tumour hypoxia.

Anxiety questionnaire

Undertaking OE-MRI in patients with HNSCC may cause greater distress than imaging in other anatomical regions due to the nature of the symptoms commonly experienced by this patient group. In addition, as hypoxic-PET imaging studies have suggested that hypoxic regions that fail to reoxygenate with treatment are a more sensitive biomarker of radioresistance [11, 13], repeated OE-MRI assessments during treatment may be beneficial [13, 43]. Although it has been demonstrated previously that OE-MRI is tolerated by patients with HNSCC [37], a formal assessment of patients' experience of the OE-MRI scan to ensure maximal tolerability and therefore willingness to undergo repeat scanning is useful.

Overall, the OE-MRI scan was well tolerated with only one participant terminating their study scan prematurely. Although anxiety scores were worse with the OE-MRI scan, the magnitude of the difference was small and of doubtful clinical significance; however, all participants voluntarily agreed to undergo a longer MRI scan and therefore potentially represent a subset of patients less prone to MRI scan anxiety. In addition, as the study sequence was performed prior to routine clinical imaging, participants may have felt more comfortable with

the MRI environment as the imaging session progressed. Further OE-MRI studies should be mindful of the potential burden additional or extended scans place on this group of patients who are undergoing an already significant amount of medical imaging during a psychologically challenging time.

Limitations

The aim of this study was to evaluate the feasibility of performing OE-MRI in suspected HNSCC in a clinical environment and not to repeat the work of previous authors in demonstrating the efficacy of OE-MRI in determining tumour hypoxia [19, 21, 25, 36, 44]. Nevertheless, histopathological correlation with a suitable hypoxia marker would have enabled comparison and evaluation of the accuracy of the estimated hypoxic fractions. In addition, at our centre, routine histological verification of malignant cervical lymph nodes is reserved for cases with equivocal radiological findings only. Without surgical treatment, no definitive histology of nodal masses is obtained hence correlation with clinical outcome in this study was limited to histologically confirmed primary tumours.

The majority of primary tumours in this study were oropharyngeal (11/15) with 82% (9/11) positive for p16 expression (high-risk HPV variant deoxyribonucleic acid detected in 7 cases) representing a likely selection bias in the patient recruitment design of the study. HPV-related cancers are relatively more radiosensitive than HPV-negative tumours, and although both types display similar levels of hypoxia [45], pharmacological hypoxia modification therapies appear less effective in HPV-positive tumours [46, 47]. The ability to stratify HPV-positive tumours based on their hypoxia status may therefore be less clinically relevant than for HPV-negative tumours.

Conclusions

We present a well-tolerated implementation of dynamic, volumetric OE-MRI in the head and neck region using routinely available equipment in an acute hospital setting that was able to discern differing responses to supplemental oxygen within biopsy-confirmed HNSCC. Further adequately powered studies are now required in HNSCC to investigate the predictive power of OE-MRI estimated tumour hypoxic fractions in discriminating patients more likely to benefit from the addition of hypoxia modification therapy to radiotherapy treatments.

Abbreviations

BOLD	Blood oxygen level-dependent
CI	Confidence interval
HNSCC	Head and neck squamous cell carcinoma
HPV	Human papillomavirus

OE-MRI	Oxygen-enhanced magnetic resonance imaging
PET	Positron emission tomography
pO ₂	Oxygen tension
VIBE	Volumetric interpolated breath-hold examination
VOI	Volume of interest

Supplementary Information

The online version contains supplementary material available at <https://doi.org/10.1186/s41747-024-00429-1>.

Additional file 1: Appendix 1. Tumour characteristics and OE-MRI derived parameters for all identified primary tumours and malignant nodal masses. **Fig. S1.** A member of the research team modelling the participant setup. The posterior component of the head coil was used together with an ultraflex large 18-channel coil positioned over the neck region allowing ready placement of the non-rebreather oxygen mask. The non-rebreather bag was positioned on top of the ultraflex coil. Study participants wore ear plugs and ear defenders and did not wear a surgical face mask during the scan. **Fig. S2.** T1 values for 12 tubes in a Eurospin TO5 phantom measured using the study dynamic vibe sequence. T1 values quoted are mean values over all 40 acquisitions. Coefficient of variations quoted for each tube have a median value of 0.2%. **Fig. S3.** Example OE-MRI parametrical maps in a patient with a suspected malignant nodal mass (patient no: 16 Lymph Node no: 2). Low estimated hypoxic fraction (11.6%) is shown on a T1 weighted vibe image with overlaid parametric $\Delta T1$ map of the malignant mass (a, d, axial and coronal plane respectively) and overlaid statistical map of $\Delta T1$ times (b, e). Blue colour indicates statistically significant decrease in T1 times, white indicating no statistically significant change and red indicating statistically significant increasing T1 times. c Time series of T1 times averaged over the entire malignant node VOI and over those voxels with significantly decreasing T1 times only. f Histogram of $\Delta T1$ times for the entire malignant nodal VOI. *OE-MRI* Oxygen-enhanced magnetic resonance imaging, *VIBE* Volumetric interpolated breath-hold examination, *VOI* Volume of interest. **Fig. S4.** Example OE-MRI parametrical maps in a patient with a suspected malignant nodal mass (patient no: 15 Lymph Node no: 7). High estimated hypoxic fraction (72.0%) is shown on a T1 weighted vibe image with overlaid parametric $\Delta T1$ map of the malignant mass (a, d, axial and coronal plane respectively) and overlaid statistical map of $\Delta T1$ times (b, e). Blue colour indicates statistically significant decrease in T1 times, white indicating no statistically significant change and red indicating statistically significant increasing T1 times. c Time series of T1 times averaged over the entire malignant node VOI and over those voxels with significantly decreasing T1 times only. f Histogram of $\Delta T1$ times for the entire malignant nodal VOI. *OE-MRI* Oxygen-enhanced magnetic resonance imaging, *VIBE* Volumetric interpolated breath-hold examination, *VOI* Volume of interest. **Supplementary Table S1.** Summed scores from all patient participants for each of the 15 domains assessed in the MRI specific anxiety questionnaire.

Acknowledgements

The authors thank Mr. Mahmoud Elsayed, Ms. Bindhu Saraswathy, and Ms. Emma Mallinder for helping with patient recruitment and the staff of Nottingham University Hospitals NHS Trust's MRI department for scanning of participants. The authors declare that no large language models were used for this manuscript including for all tables and figures.

Authors' contributions

AM had a substantial role in the conception and design of the study as well as being the principal software developer, analyst and interpreter of the data, and principal writer of the manuscript. SM contributed to the concept and design of the study. SR contributed to the design of the study and the acquisition of the imaging data. JS contributed to the design of the study and acquisition of the data and provided specialist radiologist advice. PSM contributed to the concept and design of the study as well as the acquisition of the imaging data. DB contributed to the analysis of the data and the software used. RP led on the study concept and design as well as making major contributions to data analysis and interpretation and the writing of this manuscript. All authors

read and approved the final manuscript. PSM is a member of the UK National Institute of Health Research's Nottingham Biomedical Research Centre.

Funding

This study has received funding from a grant from Nottingham University Hospitals Charity (grant number APP2361/N0379). DB is supported by the National Science Center (Poland) project No. 2020/04/X/ST6/02136.

Availability of data and materials

All data generated or analysed during this study are included in this published article and its supplementary information files.

Declarations

Ethics approval and consent to participate

Ethical approval for this study was obtained from the South Central Berkshire Research Ethics Committee (reference 21/SC/0050) on 9 February 2021. Written informed consent was obtained from all subjects in this study.

Consent for publication

Not applicable.

Competing interests

The authors declare no relationships with any companies, whose products or services may be related to the subject matter of the article.

Author details

¹Academic Unit of Translational Medical Sciences, School of Medicine, University of Nottingham, Nottingham, UK. ²Department of Clinical Oncology, Nottingham University Hospitals NHS Trust, City Hospital, Hucknall Road, Nottingham NG5 1PB, UK. ³Department of Radiology, Nottingham University Hospitals NHS Trust, Nottingham, UK. ⁴Mental Health & Clinical Neurosciences Unit, School of Medicine, University of Nottingham, Nottingham, UK. ⁵Department of Medical Physics & Clinical Engineering, Nottingham University Hospitals NHS Trust, Nottingham, UK. ⁶Department of Systems Biology and Engineering, Silesian University of Technology, Gliwice, Poland.

Received: 1 September 2023 Accepted: 8 January 2024

Published online: 06 March 2024

References

- (2015) Cancer incidence for common cancers. Cancer Research UK. <https://www.cancerresearchuk.org/health-professional/cancer-statistics/incidence>. Accessed 20 Feb 2023
- (2016) Head and neck cancers survival statistics. Cancer Research UK. <https://www.cancerresearchuk.org/health-professional/cancer-statistics/statistics-by-cancer-type/head-and-neck-cancers/survival>. Accessed 21 Feb 2023
- Brizel DM, Sibley GS, Prosnitz LR et al (1997) Tumor hypoxia adversely affects the prognosis of carcinoma of the head and neck. *Int J Radiat Oncol Biol Phys* 38:285–289. [https://doi.org/10.1016/S0360-3016\(97\)00101-6](https://doi.org/10.1016/S0360-3016(97)00101-6)
- Overgaard J (2011) Hypoxic modification of radiotherapy in squamous cell carcinoma of the head and neck—a systematic review and meta-analysis. *Radiother Oncol* 100:22–32. <https://doi.org/10.1016/j.radonc.2011.03.004>
- Hodolič M, Fettich J, Kairemo K (2015) Hypoxia PET tracers in EBRT dose planning in head and neck cancer. *Curr Radiopharm* 8:32–37. <https://doi.org/10.2174/1874471008666150316222400>
- Welz S, Paulsen F, Pfannenbergl C et al (2022) Dose escalation to hypoxic subvolumes in head and neck cancer: a randomized phase II study using dynamic [¹⁸F]FMISO PET/CT. *Radiother Oncol* 171:30–36. <https://doi.org/10.1016/j.radonc.2022.03.021>
- Busk M, Overgaard J, Horsman MR (2020) Imaging of tumor hypoxia for radiotherapy: current status and future directions. *Semin Nucl Med* 50:562–583. <https://doi.org/10.1053/j.semnuclmed.2020.05.003>
- Hughes VS, Wiggins JM, Siemann DW (2019) Tumor oxygenation and cancer therapy—then and now. *Br J Radiol* 92:20170955. <https://doi.org/10.1259/bjr.20170955>
- Huang Y, Fan J, Li Y et al (2021) Imaging of tumor hypoxia with radionuclide-labeled tracers for PET. *Front Oncol* 11:731503. <https://doi.org/10.3389/fonc.2021.731503>
- Mortensen LS, Johansen J, Kallehauge J et al (2012) FAZA PET/CT hypoxia imaging in patients with squamous cell carcinoma of the head and neck treated with radiotherapy: results from the DAHANCA 24 trial. *Radiother Oncol* 105:14–20. <https://doi.org/10.1016/j.radonc.2012.09.015>
- Zips D, Zöphel K, Abolmaali N et al (2012) Exploratory prospective trial of hypoxia-specific PET imaging during radiochemotherapy in patients with locally advanced head-and-neck cancer. *Radiother Oncol* 105:21–28. <https://doi.org/10.1016/j.radonc.2012.08.019>
- Graves EE, Hicks RJ, Binns D et al (2016) Quantitative and qualitative analysis of [¹⁸F]FDG and [¹⁸F]FAZA positron emission tomography of head and neck cancers and associations with HPV status and treatment outcome. *Eur J Nucl Med Mol Imaging* 43:617–625. <https://doi.org/10.1007/s00259-015-3247-7>
- Löck S, Perrin R, Seidlitz A et al (2017) Residual tumour hypoxia in head-and-neck cancer patients undergoing primary radiochemotherapy, final results of a prospective trial on repeat FMISO-PET imaging. *Radiother Oncol* 124:533–540. <https://doi.org/10.1016/j.radonc.2017.08.010>
- Bandurska-Luque A, Löck S, Haase R et al (2019) FMISO-PET-based lymph node hypoxia adds to the prognostic value of tumor only hypoxia in HNSCC patients. *Radiother Oncol* 130:97–103. <https://doi.org/10.1016/j.radonc.2018.09.008>
- Löck S, Linge A, Seidlitz A et al (2019) Repeat FMISO-PET imaging weakly correlates with hypoxia-associated gene expressions for locally advanced HNSCC treated by primary radiochemotherapy. *Radiother Oncol* 135:43–50. <https://doi.org/10.1016/j.radonc.2019.02.020>
- Thorwarth D, Welz S, Mönnich D et al (2019) Prospective evaluation of a tumor control probability model based on dynamic 18F-FMISO PET for head and neck cancer radiotherapy. *J Nucl Med* 60:1698–1704. <https://doi.org/10.2967/jnumed.119.227744>
- Salem A, Asselin M-C, Reyman B et al (2018) Targeting hypoxia to improve non-small cell lung cancer outcome. *J Natl Cancer Inst* 110:14–30. <https://doi.org/10.1093/jnci/djx160>
- O'Connor JPB, Naish JH, Parker GJM et al (2009) Preliminary study of oxygen-enhanced longitudinal relaxation in MRI: a potential novel biomarker of oxygenation changes in solid tumors. *Int J Radiat Oncol Biol Phys* 75:1209–1215. <https://doi.org/10.1016/j.ijrobp.2008.12.040>
- O'Connor JPB, Boulton JKR, Jamin Y et al (2016) Oxygen-enhanced MRI accurately identifies, quantifies, and maps tumor hypoxia in preclinical cancer models. *Cancer Res* 76:787–795. <https://doi.org/10.1158/0008-5472.CAN-15-2062>
- O'Connor JPB, Naish JH, Jackson A et al (2009) Comparison of normal tissue R-1 and R-2* modulation by oxygen and carbogen. *Magn Reson Med* 61:75–83. <https://doi.org/10.1002/mrm.21815>
- Salem A, Little RA, Latif A et al (2019) Oxygen-enhanced MRI is feasible, repeatable, and detects radiotherapy-induced change in hypoxia in xenograft models and in patients with non-small cell lung cancer. *Clin Cancer Res* 25:3818–3829. <https://doi.org/10.1158/1078-0432.CCR-18-3932>
- Belfatto A, White DA, Mason RP et al (2016) Tumor radio-sensitivity assessment by means of volume data and magnetic resonance indices measured on prostate tumor bearing rats. *Med Phys* 43:1275–1284. <https://doi.org/10.1118/1.4941746>
- Cao-Pham T-T, Tran L-B-A, Colliex F et al (2016) Monitoring tumor response to carbogen breathing by oxygen-sensitive magnetic resonance parameters to predict the outcome of radiation therapy: a preclinical study. *Int J Radiat Oncol Biol Phys* 96:149–160. <https://doi.org/10.1016/j.ijrobp.2016.04.029>
- Cao-Pham T-T, Joudiou N, Van Hul M et al (2017) Combined endogenous MR biomarkers to predict basal tumor oxygenation and response to hyperoxic challenge. *NMR Biomed* 30:e3836. <https://doi.org/10.1002/nbm.3836>
- Little RA, Jamin Y, Boulton JKR et al (2018) Mapping hypoxia in renal carcinoma with oxygen-enhanced MRI: comparison with intrinsic susceptibility MRI and pathology. *Radiology* 288:739–747. <https://doi.org/10.1148/radiol.2018171531>

26. Burrell JS, Walker-Samuel S, Baker LCJ et al (2013) Exploring $\Delta R(2)$ * and $\Delta R(1)$ as imaging biomarkers of tumor oxygenation. *J Magn Reson Imaging* 38:429–434. <https://doi.org/10.1002/jmri.23987>
27. O'Connor JPB, Robinson SP, Waterton JC (2019) Imaging tumour hypoxia with oxygen-enhanced MRI and BOLD MRI. *Br J Radiol* 92:20180642. <https://doi.org/10.1259/bjr.20180642>
28. Bluemke E, Stride E, Bulte DP (2022) Modeling the effect of hyperoxia on the spin-lattice relaxation rate R1 of tissues. *Magn Reson Med* 88:1867–1885. <https://doi.org/10.1002/mrm.29315>
29. Avants BB, Tustison NJ, Song G et al (2011) A reproducible evaluation of ANTs similarity metric performance in brain image registration. *Neuroimage* 54:2033–2044. <https://doi.org/10.1016/j.neuroimage.2010.09.025>
30. Fram EK, Herfkens RJ, Johnson GA et al (1987) Rapid calculation of T1 using variable flip angle gradient refocused imaging. *Magn Reson Imaging* 5:201–208. [https://doi.org/10.1016/0730-725x\(87\)90021-x](https://doi.org/10.1016/0730-725x(87)90021-x)
31. (2015) T1 & T2 EUROSPPIN Gels. Leeds Test Objects. <https://leedstestobjects.com/index.php/phantom/t1-t2-gels/>. Accessed 5 Jan 2024
32. Brouwer CL, Steenbakkers RJHM, Bourhis J et al (2015) CT-based delineation of organs at risk in the head and neck region: DAHANCA, EORTC, GORTEC, HKNPCSG, NCIC CTG, NCRI, NRG Oncology and TROG consensus guidelines. *Radiother Oncol* 117:83–90. <https://doi.org/10.1016/j.radonc.2015.07.041>
33. Yushkevich PA, Piven J, Cody Hazlett H et al (2006) User-guided 3D active contour segmentation of anatomical structures: significantly improved efficiency and reliability. *Neuroimage* 31:1116–1128
34. Ahlander BM, Årestedt K, Engvall J et al (2016) Development and validation of a questionnaire evaluating patient anxiety during Magnetic Resonance Imaging: the Magnetic Resonance Imaging-Anxiety Questionnaire (MRI-AQ). *J Adv Nurs* 72:1368–1380. <https://doi.org/10.1111/jan.12917>
35. Machiels J-P, René Leemans C, Golusinski W et al (2020) Squamous cell carcinoma of the oral cavity, larynx, oropharynx and hypopharynx: EHNES-ESMO-ESTRO Clinical Practice Guidelines for diagnosis, treatment and follow-up. *Ann Oncol* 31:1462–1475. <https://doi.org/10.1016/j.annonc.2020.07.011>
36. Linnik IV, Scott MLJ, Holliday KF et al (2014) Noninvasive tumor hypoxia measurement using magnetic resonance imaging in murine U87 glioma xenografts and in patients with glioblastoma. *Magn Reson Med* 71:1854–1862. <https://doi.org/10.1002/mrm.24826>
37. Dubec MJ, Buckley DL, Berks M et al (2023) First-in-human technique translation of oxygen-enhanced MRI to an MR Linac system in patients with head and neck cancer. *Radiother Oncol* 183:109592. <https://doi.org/10.1016/j.radonc.2023.109592>
38. Bluemke E, Bertrand A, Chu K-Y et al (2023) Oxygen-enhanced MRI and radiotherapy in patients with oropharyngeal squamous cell carcinoma. *Clin Transl Radiat Oncol* 39:100563. <https://doi.org/10.1016/j.ctro.2022.100563>
39. McCabe A, Martin S, Shah J et al (2023) T1 based oxygen-enhanced MRI in tumours; a scoping review of current research. *Br J Radiol* 96:20220624. <https://doi.org/10.1259/bjr.20220624>
40. O'Connor JPB, Aboagye EO, Adams JE et al (2017) Imaging biomarker roadmap for cancer studies. *Nat Rev Clin Oncol* 14:169–186. <https://doi.org/10.1038/nrclinonc.2016.162>
41. Shukla-Dave A, Obuchowski NA, Chenevert TL et al (2019) Quantitative imaging biomarkers alliance (QIBA) recommendations for improved precision of DWI and DCE-MRI derived biomarkers in multicenter oncology trials. *J Magn Reson Imaging* 49:e101–e121. <https://doi.org/10.1002/jmri.26518>
42. Vaupel P, Hoeckel M, Mayer A (2007) Detection and characterization of tumor hypoxia using pO(2) histography. *Antioxid Redox Signal* 9:1221–1235. <https://doi.org/10.1089/ars.2007.1628>
43. Martens RM, Noij DP, Ali M et al (2019) Functional imaging early during (chemo)radiotherapy for response prediction in head and neck squamous cell carcinoma; a systematic review. *Oral Oncol* 88:75–83. <https://doi.org/10.1016/j.oraloncology.2018.11.005>
44. White DA, Zhang Z, Li L et al (2016) Developing oxygen-enhanced magnetic resonance imaging as a prognostic biomarker of radiation response. *Cancer Lett* 380:69–77. <https://doi.org/10.1016/j.canlet.2016.06.003>
45. Göttgens E-L, Ostheimer C, Span PN et al (2019) HPV, hypoxia and radiation response in head and neck cancer. *Br J Radiol* 92:20180047. <https://doi.org/10.1259/bjr.20180047>
46. Lassen P, Eriksen JG, Hamilton-Dutoit S et al (2010) HPV-associated p16-expression and response to hypoxic modification of radiotherapy in head and neck cancer. *Radiother Oncol* 94:30–35. <https://doi.org/10.1016/j.radonc.2009.10.008>
47. Rischin D, Young RJ, Fisher R et al (2010) Prognostic significance of p16INK4A and human papillomavirus in patients with oropharyngeal cancer treated on TROG 02.02 phase III trial. *J Clin Oncol* 28:4142–4148. <https://doi.org/10.1200/JCO.2010.29.2904>

Publisher's Note

Springer Nature remains neutral with regard to jurisdictional claims in published maps and institutional affiliations.